

## SOLVING THE GRADIOMETRIC BOUNDARY VALUE PROBLEM BY THE FINITE ELEMENT METHOD\*

MAREK MACÁK , KAROL MIKULA , ZUZANA MINARECHOVÁ , AND RÓBERT  
ČUNDERLÍK †

**Abstract.** We present an innovative numerical approach for gravity field modelling where the second derivatives of disturbing potential measured at the level of satellite orbits can be directly taken into account. To that goal, we create the computational domain bounded by the chosen region on the Earth’s surface, corresponding boundary at the level of chosen satellites and additional four side boundaries. The boundary value problem consists of the Laplace equation for the unknown disturbing potential accompanied by the first derivatives of the disturbing potential given on the approximation of the Earth’s surface, the second derivatives of the disturbing potential, e.g. from the GOCE measurements, given on the upper boundary away from the Earth, and the disturbing potential given on four side boundaries. To solve such a problem, we have derived the numerical scheme based on the finite element and the finite difference methods. We test its order of convergence by one theoretical experiment, and then we present gravity field modelling in Europe using EGM2008 data.

**Key words.** The second-order vertical (radial) potential derivatives as boundary conditions, Gravity field modelling.

**AMS subject classifications.** 35J25, 65N30, 65N06

**1. Introduction.** Modeling the Earth’s gravity field using gradiometry data has been of interest for many researchers, see, e.g., R. Rummel and O. L. Colombo [22], Holota [10], Tscherning et al. [25], Brovelli et al. [4], Luo [14], Eshagh [6], Šprlák et al. [24] or Novák et al. [19], and references therein. In our approach, we will apply the finite element method (FEM), see Brenner and Scott [3] or Reddy [21], for solving the gradiometric boundary value problem (BVP). The FEM has been applied to gravity field modelling for the first time by Meissl [17] and Shaofeng and Dingbo [23], and later by Fašková et al. [7, 8]. Recently, Yin and Sneeuw published an approach to the gravitational field modelling by using CFD (Computational Fluid Dynamics) techniques [26], and Macák et al. [15] and Minarechová et al. [18] applied the FEM approaches for solving the oblique derivative BVP in local domains.

In this paper, we continue in our previous studies [7, 8, 15, 18], but instead of the Dirichlet BC prescribed at the satellites orbits we suppose the second-order vertical (radial) disturbing potential derivatives. Our main motivation for this change is to use the filtered satellite gradiometry data directly measured by the mission GOCE, see, e.g., [5]. To derive the numerical scheme, we implement the FEM with the finite difference method (FDM). Finally, we present a numerical experiment with EGM2008 in the Europe.

---

\*This work was supported by Grant No.: APVV-19-0460, APVV-23-0186 and VEGA 1/0690/24.

†Faculty of Civil Engineering, Slovak University of Technology, Radlinského 11, 810 05 Bratislava, Slovak Republic, (marek.macak@stuba.sk, karol.mikula@stuba.sk, zuzana.minarechova@stuba.sk, cunderli@svf.stuba.sk).



**3. Solution to the BVP by the FEM.** In our approach, we follow the fundamental principles of FEM published by Reddy in [21].

**3.1. Discretization of the computational domain.** The FEM assumes discretization of the whole computational domain  $\Omega$  by a union of elements  $\Omega^e$ ,  $e = 1, \dots, \mathcal{N}$ , where  $\mathcal{N}$  denotes the number of elements in the domain  $\Omega$ . Since our computations include the real Earth's surface and we approximate it by a series of triangles, we choose pentahedral elements with triangular base, see e.g. [16].

We divide the computational domain  $\Omega$  into  $n_1$ ,  $n_2$ ,  $n_3$  divisions in latitudinal, longitudinal and vertical (radial) direction, respectively, to create the spherical prisms - tesseroids. Then we diagonally cut each tesseroid to create  $(2 \times n_1) \times (2 \times n_2) \times n_3$  triangular prisms, i.e., pentahedral elements. To specify the position of an element  $\Omega^e$  we use indexes  $k, l, m$ , where  $k = 1, \dots, 2n_1$ ,  $l = 1, \dots, 2n_2$  and  $m = 1, \dots, n_3$ .

**3.2. Derivation of the weak formulation on the element.** Let us consider an arbitrary element  $\Omega^e$  from our finite element discretization. We multiply the differential equation (2.1) by a weight function  $w$  and using Green's identity (we omit  $(\mathbf{x})$  to simplify the notation in the following equations) we obtain the weak formulation of (2.1) over an above defined element  $\Omega^e$ ,  $e = 1, \dots, \mathcal{N}$

$$\int_{\Omega^e} \nabla T \cdot \nabla w \, dx dy dz = \int_{\partial\Omega^e} \nabla T \cdot \mathbf{n} w \, d\sigma, \quad (3.1)$$

where  $\mathbf{n}$  denotes the unit normal to  $\partial\Omega^e$ .

Since on the bottom boundary  $\Gamma$  the oblique derivative BC (2.5) is prescribed, for the row of elements that lie on this boundary, i.e.,  $k = 1, \dots, 2n_1$ ,  $l = 1, \dots, 2n_2$  and  $m = 1$ , we modify (3.1) in the following way. We split the oblique vector  $\mathbf{s}$  into one normal and two tangential components

$$\mathbf{s} = c_1 \mathbf{n} + c_2 \mathbf{t}_1 + c_3 \mathbf{t}_2, \quad (3.2)$$

where  $\mathbf{n}$  is the normal vector and  $\mathbf{t}_1, \mathbf{t}_2$  are tangent vectors to  $\Gamma^e \subset \partial\Omega^e \subset R^3$ , where  $\Gamma^e$  denotes the bottom boundary of an element  $\Omega^e$ .

Then we replace vector  $\mathbf{s}$  in (2.5) by (3.2) to obtain

$$\nabla T \cdot \mathbf{s} = c_1 \nabla T \cdot \mathbf{n} + c_2 \nabla T \cdot \mathbf{t}_1 + c_3 \nabla T \cdot \mathbf{t}_2 = -\delta g. \quad (3.3)$$

From (3.3) we express the normal derivative

$$\nabla T \cdot \mathbf{n} = \frac{-\delta g}{c_1} - \frac{c_2}{c_1} \frac{\partial T}{\partial \mathbf{t}_1} - \frac{c_3}{c_1} \frac{\partial T}{\partial \mathbf{t}_2}, \quad (3.4)$$

where we assume that  $c_1 \neq 0$ .

Now, we insert (3.4) to (3.1) to get

$$\begin{aligned} & \int_{\Omega^e} \nabla T \cdot \nabla w \, dx dy dz = \\ & = \int_{\Gamma^e} \left( \frac{-\delta g}{c_1} - \frac{c_2}{c_1} \frac{\partial T}{\partial \mathbf{t}_1} - \frac{c_3}{c_1} \frac{\partial T}{\partial \mathbf{t}_2} \right) w \, d\sigma + \int_{\partial\Omega^e \setminus \Gamma^e} \nabla T \cdot \mathbf{n} w \, d\sigma. \end{aligned} \quad (3.5)$$

After some rearrangement, we have

$$\begin{aligned} & \int_{\Omega^e} \nabla T \cdot \nabla w \, dx dy dz + \frac{c_2}{c_1} \int_{\Gamma^e} \frac{\partial T}{\partial \mathbf{t}_1} w \, d\sigma + \frac{c_3}{c_1} \int_{\Gamma^e} \frac{\partial T}{\partial \mathbf{t}_2} w \, d\sigma = \\ & = \int_{\Gamma^e} \frac{-\delta g}{c_1} w \, d\sigma + \int_{\partial\Omega^e \setminus \Gamma^e} \nabla T \cdot \mathbf{n} w \, d\sigma. \end{aligned} \quad (3.6)$$

In this way, we have obtained the weak formulation (3.1) or (3.6) of the BVP (2.1) - (2.3) on every element  $\Omega^e$ . The study of weak solution of the oblique derivative BVP is included in the book by Lieberman [13].

**3.3. Solution by the Finite Element Method.** For a pentahedral element  $\Omega^e$  with six nodes, we can write

$$T \approx T^e = \sum_{j=1}^6 T_j^e \psi_j(x, y, z), \quad (3.7)$$

i.e. we take an approximation of the unknown value  $T$  as  $T^e$ , a linear combination of basis functions  $\psi_j$  with coefficients  $T_j^e$ ,  $j = 1, \dots, 6$ . Then we substitute it into the weak formulation (3.1) for elements  $\Omega^e$  with indexes  $k = 1, \dots, 2n_1$ ,  $l = 1, \dots, 2n_2$  and  $m = 2, \dots, n_3$ , and consider  $\psi_i$  for weight function  $w$ . We obtain the  $i^{th}$  equation in the form

$$\begin{aligned} & \sum_{j=1}^6 T_j^e \int_{\Omega^e} \frac{\partial \psi_j}{\partial x} \frac{\partial \psi_i}{\partial x} + \frac{\partial \psi_j}{\partial y} \frac{\partial \psi_i}{\partial y} + \frac{\partial \psi_j}{\partial z} \frac{\partial \psi_i}{\partial z} \, dx dy dz = \\ & = \sum_{j=1}^6 \int_{\partial\Omega^e} q_n \psi_i \, dx dy, \end{aligned} \quad (3.8)$$

where  $q_n = \nabla T \cdot \mathbf{n}$  denotes the projection of the vector  $\nabla T$  along the unit normal  $\mathbf{n}$ .

For the row of elements  $\Omega^e$  given by indexes  $k = 1, \dots, 2n_1$ ,  $l = 1, \dots, 2n_2$  and  $m = 1$ , we follow the same way and after inserting (3.7) into (3.6) and considering  $w = \psi_i$ , we obtain the  $i^{th}$  equation in the form

$$\begin{aligned} & \sum_{j=1}^6 T_j^e \left( \int_{\Omega^e} \frac{\partial \psi_j}{\partial x} \frac{\partial \psi_i}{\partial x} + \frac{\partial \psi_j}{\partial y} \frac{\partial \psi_i}{\partial y} + \frac{\partial \psi_j}{\partial z} \frac{\partial \psi_i}{\partial z} \, dx dy dz \right) + \\ & + \sum_{j=1}^3 T_j^e \left( \frac{c_2}{c_1} \int_{\Gamma^e} \frac{\partial \psi_j}{\partial \mathbf{t}_1} \psi_i \, dx dy + \frac{c_3}{c_1} \int_{\Gamma^e} \frac{\partial \psi_j}{\partial \mathbf{t}_2} \psi_i \, dx dy \right) = \\ & = \sum_{j=1}^3 \int_{\Gamma^e} \frac{-\delta g_j}{c_1} \psi_i \, dx dy + \sum_{j=1}^6 \int_{\partial\Omega^e \setminus \Gamma^e} q_n \psi_i \, dx dy, \end{aligned} \quad (3.9)$$

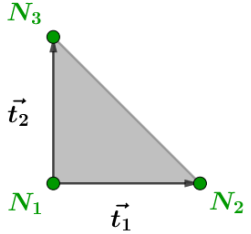
where the index  $j = 1, \dots, 3$  refers to nodes of the element  $\Omega^e$  that lie on the bottom boundary  $\Gamma$  of the computational domain  $\Omega$ . As we can see in Eq. (3.9), there are 2 tangent vectors corresponding to the nodes lying on the bottom boundary of the element belonging to  $\Gamma$ .

Now we can write (3.8) and (3.9) in a compact matrix form

$$\mathbf{K}^e \mathbf{T}^e = \mathbf{Q}^e, \quad (3.10)$$

where  $\mathbf{K}^e = [K_{ij}]$  denotes an element stiffness matrix,  $\mathbf{T}^e = (T_1, \dots, T_8)$  is a column vector of unknowns and  $\mathbf{Q}^e$  denote the right-hand side vector.

To evaluate element matrices and vectors we proceed as follows. We choose one basis function  $\psi_i$  per vertex  $N_i^e$ . Then the function  $\psi_i$  is uniquely determined by choosing value 1 at  $N_i^e$  and 0 at every  $N_j^e, i \neq j$ , and we differentiate the basis functions with respect to a position of each node in Cartesian coordinates. For more details about basis functions see, e.g., [21] or [3]. To calculate two integrals over a boundary  $\Gamma^e$  in Eq. (3.9) which include a tangential derivative, we approximate derivatives in tangential direction like in the FDM, i.e. using values of basis functions at nodes  $N_i$  of element  $e$  we have



$$\frac{\partial \psi_j^{(e)}}{\partial \mathbf{t}_1} \approx \frac{\psi_j^{(e)}(N_2) - \psi_j^{(e)}(N_1)}{d(N_1, N_2)}, \quad (3.11)$$

$$\frac{\partial \psi_j^{(e)}}{\partial \mathbf{t}_2} \approx \frac{\psi_j^{(e)}(N_3) - \psi_j^{(e)}(N_1)}{d(N_1, N_3)}, \quad (3.12)$$

where  $d$  denotes the distance between two neighbouring nodes.

**3.4. Assembly of element equations.** We assemble all element equations by using two principles:

- (i) continuity of primary variables at the interelement nodes. It means that nodal values  $T_j^e$  and  $T_j^{e+1}$  of two adjacent elements  $\Omega^e$  and  $\Omega^{e+1}$  at the connecting nodes have to be the same.
- (ii) "equilibrium" or "balance" equations of secondary variables at the interface between two elements. It means that on portions of  $\partial\Omega^e$  that are in the interior of the domain  $\Omega$ , the value  $q_n^e$  on the side  $p$  of the element  $\Omega^e$  cancels with the value  $q_n^{e+1}$  on the side  $r$  of the element  $\Omega^{e+1}$  when sides  $p$  of the element  $\Omega^e$  and  $r$  of the element  $\Omega^{e+1}$  are the same.

In this way we have obtained the global linear system of equations with a column vector of unknown global nodal values  $\mathbf{T}$

$$\mathbf{KT} = \mathbf{Q}, \quad (3.13)$$

where the matrix  $\mathbf{K}$  is sparse, since most of its entries are zero and positive definite, and the column vector  $\mathbf{Q}$  whose entries are also almost zero except for the nodes with prescribed oblique derivative BC (2.5).

**3.5. Implementing the second derivatives.** Finally, we implement the second derivatives  $T_{zz(SAT)}(\mathbf{x})$  in Eq. (2.6). In order not to reduce the accuracy of the above-defined approach, we use a second-order accurate approximation with 4-points backward differences (see Fig. 3.1)

$$\frac{\partial^2 T}{\partial \mathbf{n}^2} \approx \frac{2T_{n_3} - 5T_{n_3-1} + 4T_{n_3-2} - T_{n_3-3}}{d^2}, \quad (3.14)$$

where  $d$  denotes the distance between two neighbouring nodes and  $T_{n_3-i}$  numerical solution at them. We add these equations to (3.13) and solve the linear system of equations.

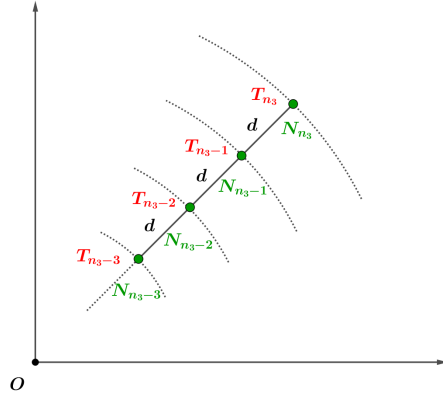


FIG. 3.1. Illustration of the numerical scheme for the approximation of the second radial derivatives given at nodes on the upper boundary  $\Gamma_U$  using 4-points backward differences, where values  $T_{n_3-i}$  denote approximation of the solution  $T$  at corresponding nodes  $N_{n_3-i}$  and  $d$  denotes the distance between two neighbouring nodes.

**4. Numerical experiments.** In the numerical experiments, we test the stability and behaviour of the numerical scheme given by (3.8) - (3.14) by investigating its Experimental Order of Convergence (EOC), and then we perform experiments with gravity data generated from EGM2008.

**4.1. Theoretical numerical experiments.** In the first experiment, the computational domain was a tesseroid bounded by  $[1, 2] \times [0, \frac{\pi}{2}] \times [\frac{\pi}{4}, \frac{3\pi}{4}]$ . The exact solution and the Dirichlet BC applied on the side boundary was given as  $T(x) = 1/r$ . The Neumann BC prescribed on the bottom boundary was  $\frac{\partial T(x)}{\partial r} = -1/r^2$  and on the upper spherical boundary we have  $\frac{\partial^2 T(x)}{\partial r^2} = \frac{2}{r^3}$ . The statistics of residuals for successive refinements of the grid can be seen in Table 4.1. For a comparison we also present the solution with the Dirichlet BC applied on the upper boundary, see Table 4.1 the first row. Although the  $L_2(\Omega)$  norm is better in the case of the experiment with Dirichlet BC,  $L_2(\Gamma_B)$  norm is very similar, and both approaches are of second order, see the EOC columns.

| BC on $\Gamma_U$  | No. of nodes | $L_2(\Omega)$ Norm | EOC   | $L_2(\Gamma_B)$ Norm | EOC   |
|-------------------|--------------|--------------------|-------|----------------------|-------|
| Dirichlet         | 4x4x4        | 0.002046           | -     | 0.000267             | -     |
|                   | 8x8x8        | 0.000370           | 2.465 | 0.000063             | 2.075 |
|                   | 16x16x16     | 0.000074           | 2.324 | 0.000015             | 2.113 |
|                   | 32x32x32     | 0.000016           | 2.184 | 0.000003             | 2.074 |
|                   | 64x64x64     | 0.000004           | 2.096 | 0.000001             | 2.041 |
| Second derivative | 4x4x4        | 0.016362           | -     | 0.000188             | -     |
|                   | 8x8x8        | 0.001325           | 3.626 | 0.000051             | 1.880 |
|                   | 16x16x16     | 0.000223           | 2.573 | 0.000012             | 2.047 |
|                   | 32x32x32     | 0.000047           | 2.242 | 0.000003             | 2.050 |
|                   | 64x64x64     | 0.000011           | 2.112 | 0.000001             | 2.031 |

TABLE 4.1

Theoretical numerical experiment:  $L_2$  norms and EOC.

**4.2. Continental gravity field modelling in a part of Europe.** In the second experiment, we have chosen a part of Europe bounded by meridians 0 deg and 30 deg, and parallels 35 deg and 55 deg. To create the bottom boundary we have used the heights generated from SRTM30 PLUS digital elevation model [1]. The height of the upper boundary  $\Gamma_U$  was at 240 km above the reference ellipsoid which corresponds to the mean altitude of the GOCE satellites. We have created four computational grids with the number of nodes  $n_1 \times n_2 \times n_3$ , namely  $225 \times 150 \times 25$ ,  $450 \times 300 \times 50$ ,  $900 \times 600 \times 100$  and  $1800 \times 1200 \times 200$ , corresponding to resolution  $8' \times 8' \times 9.6 \text{ km}$ ,  $4' \times 4' \times 4.8 \text{ km}$ ,  $2' \times 2' \times 2.4 \text{ km}$  and  $1' \times 1' \times 1.2 \text{ km}$ , respectively. All BCs were generated from global gravitational model EGM2008 based on spherical harmonics [20]. The obtained numerical solution on  $\Gamma_B$ , see Fig. 4.1, was compared with the disturbing potential generated from EGM2008 directly. Such differences are depicted in Fig. 4.2 with the corresponding statistics in Tab. 4.2. The differences on  $\Gamma_U$  are depicted in Fig. 4.3 with the statistics of residuals presented in Tab. 4.3. We have also performed the equivalent numerical experiment with the Dirichlet BC applied on  $\Gamma_U$  and compared this solution with the solution to the BVP (2.4) - (2.7). These differences are depicted in Fig. 4.4. One can observe a systematic trend in the differences on the upper boundary  $\Gamma_U$ , see Fig. 4.3, which is also obvious on the bottom boundary  $\Gamma_B$ , see Fig. 4.4. As we have expected, this trend is more dominant on the upper boundary than on the bottom one, and on both boundaries, it is significantly reduced when refining the computational grid.

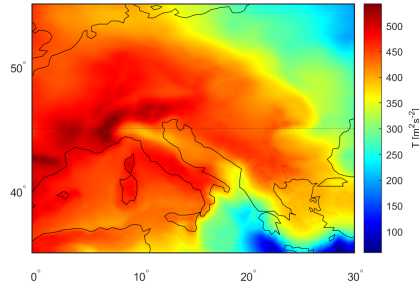


FIG. 4.1. The disturbing potential solution  $T$  on the bottom boundary  $\Gamma_B$ .

| No. of elements               | <i>Min</i> | <i>Max</i> | <i>Mean</i> | <i>Median</i> | STD   |
|-------------------------------|------------|------------|-------------|---------------|-------|
| $225 \times 150 \times 25$    | -2.938     | 7.025      | 0.009       | 0.025         | 0.372 |
| $450 \times 300 \times 50$    | -1.217     | 1.794      | 0.001       | 0.020         | 0.132 |
| $900 \times 600 \times 100$   | -0.491     | 0.386      | -0.001      | 0.015         | 0.096 |
| $1800 \times 1200 \times 200$ | -0.420     | 0.187      | -0.001      | 0.014         | 0.093 |

TABLE 4.2

Continental gravity field modelling in Europe - statistics of residuals on  $\Gamma_B$ .

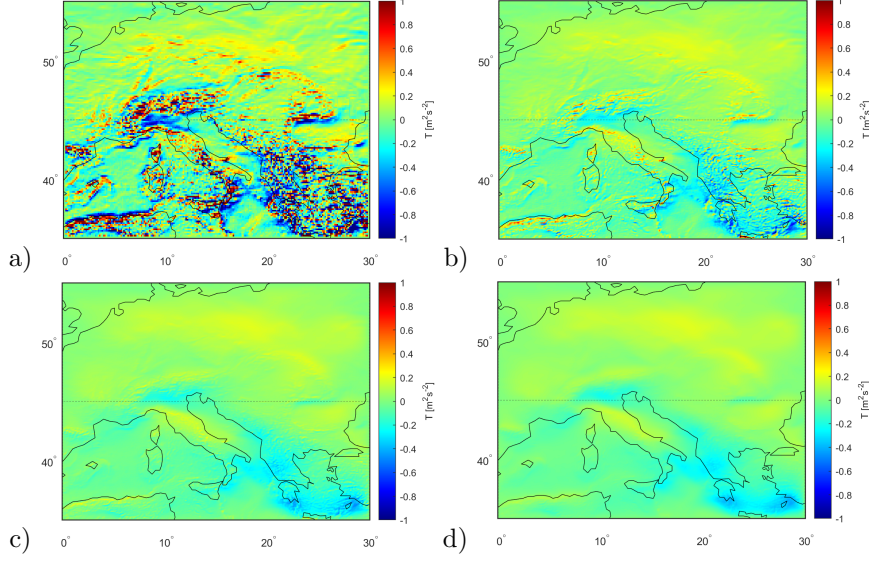


FIG. 4.2. The differences between the numerical solution to the BVP (2.4) - (2.7) and the disturbing potential generated from EGM2008 directly on the bottom boundary  $\Gamma_B$  for grids: a)  $225 \times 150 \times 25$ , b)  $450 \times 300 \times 50$ , c)  $900 \times 600 \times 100$ , d)  $1800 \times 1200 \times 200$ .

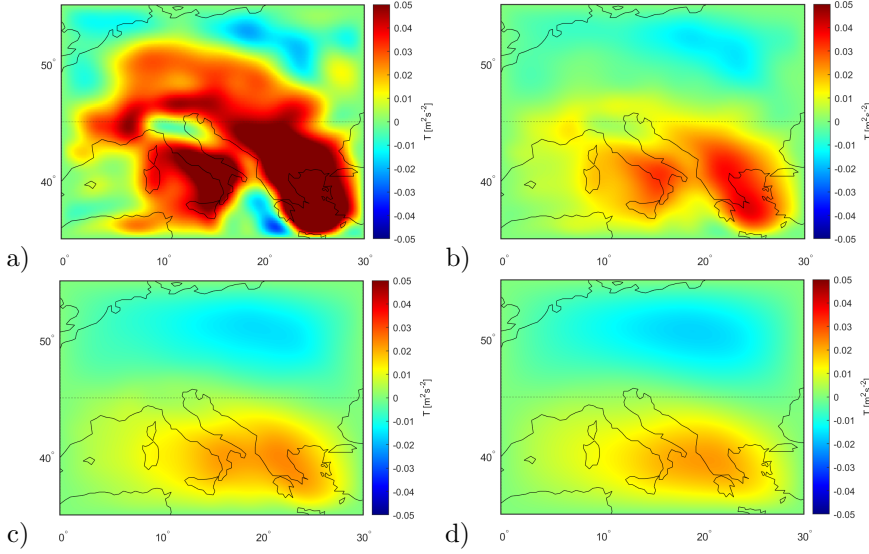


FIG. 4.3. The differences between the numerical solution to the BVP (2.4) - (2.7) and the disturbing potential generated from EGM2008 directly on the upper boundary  $\Gamma_U$  for grids: a)  $225 \times 150 \times 25$ , b)  $450 \times 300 \times 50$ , c)  $900 \times 600 \times 100$ , d)  $1800 \times 1200 \times 200$ .

**5. Summary and conclusions.** We have presented a numerical approach to gravity field modelling where the second-order vertical disturbing potential derivatives applied on the top boundary were taken into account. To derive the numerical scheme, we have implemented the finite element and the finite difference methods. At first, the proposed approach has been tested by the experiment on the unit sphere and we have shown its second order accuracy. We have compared the obtained so-



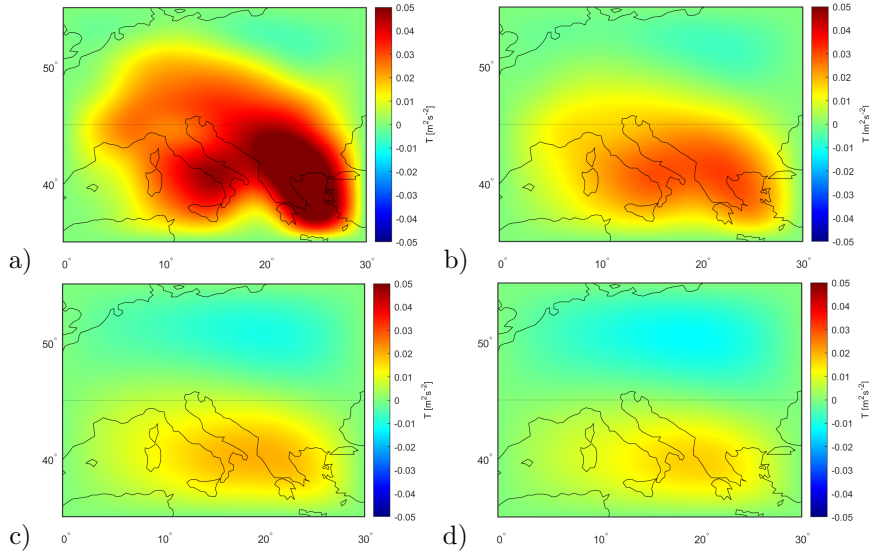


FIG. 4.4. The differences between the numerical solution with the Dirichlet BC applied on  $\Gamma_U$  and the solution to the BVP (2.4) - (2.7) on the bottom boundary  $\Gamma_B$  for grids: a)  $225 \times 150 \times 25$ , b)  $450 \times 300 \times 50$ , c)  $900 \times 600 \times 100$ , d)  $1800 \times 1200 \times 200$ .

| No. of elements               | <i>Min</i> | <i>Max</i> | <i>Mean</i> | <i>Median</i> | STD   |
|-------------------------------|------------|------------|-------------|---------------|-------|
| $225 \times 150 \times 25$    | -2.938     | 7.025      | 0.009       | 0.025         | 0.372 |
| $450 \times 300 \times 50$    | -0.015     | 0.040      | 0.005       | 0.003         | 0.011 |
| $900 \times 600 \times 100$   | -0.015     | 0.024      | 0.001       | 0.000         | 0.009 |
| $1800 \times 1200 \times 200$ | -0.015     | 0.022      | 0.000       | 0.000         | 0.009 |

TABLE 4.3

Continental gravity field modelling in Europe - statistics of residuals on  $\Gamma_U$ .

lution with the solution of the equivalent numerical experiment with the Dirichlet BC applied on the top boundary. Although the  $L_2$  norm of residuals in the whole domain was better in the case of the experiment with Dirichlet BC, the  $L_2$  norm of residuals on the bottom boundary was very similar. Afterwards, we have performed an experiment with EGM2008 data. In this case, we have observed a systematic effect when comparing the obtained solution to the solution of the corresponding experiment with the Dirichlet BC considered on the top boundary. However, this effect was significantly reduced and finally almost vanished while refining the computational grid. This experiment has shown that with a sufficiently fine grid we are able to obtain the same quality results on the bottom boundary as when applying the disturbing potential on the top boundary. In the future, we plan to perform a numerical experiment using pre-processed filtered data obtained during the last 10 months of the GOCE mission, and focus on the uniqueness of the solution in this combination of boundary conditions.

#### REFERENCES

- [1] J. J. BECKER, D. T. SANDWELL, W. H. F. SMITH, J. BRAUD, B. BINDER, J. DEPNER, D. FABRE, J. FACTOR, S. INGALLS, S.H. KIM, R. LADNER, K. MARKS, S. NELSON, A. PHARAOH, R.

- TRIMMER, J. VON ROSENBERG, G. WALLACE AND P. WEATHERALL, *Global Bathymetry and Elevation Data at 30 Arc Seconds Resolution: SRTM30 PLUS*, in *Marine Geodesy*, 32,4, 355-371, (2009).
- [2] A. BJERHAMMAR AND L. SVENSSON, *On the geodetic boundary value problem for a fixed boundary surface, A satellite approach*, *Bull Geod.*, 57 (1-4), 382-393, (1983).
- [3] S. C. BRENNER AND L. R. SCOTT, *The mathematical theory of finite element methods*, Springer-Verlag, New York, (2002).
- [4] M. BROVELLI, F. MIGLIACCIO AND F. SANSÓ, *A BVP Approach to the Reduction of Spaceborne Gradiometry: Theory and Simulations*, *LAG 110*:169–180, (1991).
- [5] R. ČUNDERLÍK, M. KOLLÁR AND K. MIKULA, *1D along-track pre-processing of the GOCE gravity gradients and nonlinear filtering of the radial components  $V_{zz}$  in spatial domain*, *Contributions to Geophysics and Geodesy*, 53(4), 333-351, (2023).
- [6] M. ESHAGH, *Alternative expression for gravity gradients in local north-oriented frame and tensor spherical harmonics*, *Acta Geophysica*, Vol. 58, 215-243, (2010).
- [7] Z. FASKOVÁ, R. ČUNDERLÍK, J. JANÁK, K. MIKULA AND M. ŠPRLÁK, *Gravimetric quasigeoid in Slovakia by the finite element method*, *Kybernetika*, Vol. 43, No. 6: 789-796, (2007).
- [8] Z. FASKOVÁ, R. ČUNDERLÍK AND K. MIKULA, *Finite element method for solving geodetic boundary value problems*, *J Geod* 84(2): 135-144, (2010).
- [9] R. FLOBERGHAGEN, M. FEHRINGER, D. LAMARRE, D. MUZI, B. FROMMKNECHT, CH. STEIGER, J. PINEIRO, AND A. DA COSTA, *Mission design, operation and exploitation of the gravity Field and steady-state ocean circulation explorer mission*, *J. Geod.*, vol. 85, 749-758, (2011).
- [10] P. HOLOTA, *Boundary Value Problems and Invariants of the Gravitational Tensor in Satellite Gradiometry*, *Lecture Notes in Earth Sciences*, Vol. 25, 447–457, (1986).
- [11] P. HOLOTA, *Coerciveness of the linear gravimetric boundary-value problem and a geometrical interpretation*, *J Geod* 71: 640-651, (1997).
- [12] K. R. KOCH AND A. J. POPE, *Uniqueness and existence for the geodetic boundary value problem using the known surface of the earth*, *Bull. Geod.*, 46, 467-476, (1972).
- [13] G. M. LIEBERMAN, *Oblique Derivative Problems for Elliptic Equations*, World Scientific Publishing Co. Pte. Ltd., Hackensack, NJ, ISBN: 978-981-4452-32-8, (2013).
- [14] Z. C. LUO, *The Theory and Methodology for the Determination of the Earth's Gravity Field from Satellite Gravity Gradiometry Data*, Dissertation (in Chinese), Wuhan Technical University of Surveying and Mapping, (1996).
- [15] M. MACÁK, Z. MINARECHOVÁ, R. ČUNDERLÍK AND K. MIKULA, *The finite element method as a tool to solve the oblique derivative boundary value problem in geodesy*, *Tatra Mountains Mathematical Publications*. Vol. 75, no. 1, 63-80, (2020).
- [16] M. MACÁK, Z. MINARECHOVÁ, L. TOMEK, R. ČUNDERLÍK AND K. MIKULA, *Solving the fixed gravimetric boundary value problem by the finite element method using mapped infinite elements*, *Computational Geosciences*, (2023).
- [17] P. MEISSL, *The use of finite elements in physical geodesy*, Report 313, Geodetic Science and Surveying, The Ohio State University, (1981).
- [18] Z. MINARECHOVÁ, M. MACÁK, R. ČUNDERLÍK AND K. MIKULA, *On the finite element method for solving the oblique derivative boundary value problems and its application in local gravity field modelling*, *Journal of Geodesy*, Vol. 95, 70, (2021).
- [19] P. NOVÁK, M. ŠPRLÁK AND M. PITOŇÁK, *On determination of the geoid from measured gradients of the Earth's gravity field potential*, *Earth-Science Reviews*, Vol. 221, 103773, (2021).
- [20] N. K. PAVLIS, S. A. HOLMES, S. C. KENYON AND J. K. FACTOR, *The development and evaluation of the Earth Gravitational Model 2008 (EGM2008)*, *Journal of Geophysical Research*, 117, B04406, (2012).
- [21] J. N. REDDY, *An Introduction to the Finite Element Method, 3rd Edition*, McGraw-Hill Education, New York, ISBN: 9780072466850, (2006).
- [22] R. RUMMEL AND O. L. COLOMBO, *Gravity Field Determination from Satellite Gradiometry*, *Bulletin Geodesique* 57, 233–246, (1985).
- [23] B. SHAOFENG AND C. DINGBO, *The finite element method for the geodetic boundary value problem*, *Manuscr Geod* 16:353–359, (1991).
- [24] M. ŠPRLÁK, J. SEBERA, M. VAĽKO AND P. NOVÁK, *Spherical integral formulas for upward/downward continuation of gravitational gradients onto gravitational gradients*, *Journal of Geodesy*, Vol. 88, 2, 179-197, (2014).
- [25] C. C. TSCHERNING, R. FORSBERG AND M. VERMEER, *Methods for Regional Gravity Field Modelling from SST and SGG Data*, Report 90: 2, Finnish Geodetic Institute, Helsinki, (1990).
- [26] Z. YIN AND N. SNEEUW, *Modeling the gravitational field by using CFD techniques*, *J Geod* 95, 68 (2021).